Sule Lamido University Journal of Science and Technology (SLUJST) Vol. 2 No. 2 [June, 2021], pp. 96-103

Ligand Field Parameters of Neodymium Activated Lithium Strontium Zinc Borate Glasses

Ahmad Umar Ahmad[a]
[a]Integrated Science Department, Jigawa State College of Education PMB 1002, Gumel, Jigawa State, Nigeria

Abstract

Nd_2O_3 activated borate-based glass series of molar composition of $20Li_2CO_3$–5SrO–5ZnO–(70-x)B_2O_3–xNd_2O_3 ($0 \leq x \leq 2$) was prepared via conventional melt quenching procedure. The prepared glass samples were characterized to evaluate the influence of Nd_2O_3 activation on their optical absorbance, ligand and crystal field parameter, as well as optical band gap energy. The XRD spectra of the glass samples depict a wide hump in the range of $15^o - 38^o$ which infer their amorphous nature. The EDX analysis of the glasses detected the right traced elemental compositions. The spectra of the optical absorption of the glasses disclosed twelve unambiguous absorptions peaks with hypersensitive band at 17212 cm^{-1}. The bandgaps and Urbach energies of the glasses were found to be sensitive to the variation in Nd_2O_3 contents. The first three optical absorption bands near the UV edge were used to evaluate the ligand field parameters. The calculated Racah parameters (B and C) of the glasses indicated a reasonable change in the inter-electronic repulsion with the increase in Nd_2O_3 dopant concentrations. The alteration in the crystal field parameters (Dq and Dq/B) of glasses with Nd_2O_3 activation displayed a rise in the degree of covalency.

Keywords: *Borate based glass, Neodymium, Optical absorption spectra, DASF, Nephelauxetic ratio*

1. Introduction

Glasses and Crystals activated with Trivalent rare-earth ions (REIs) have been extensively researched owing to their applications in photonic devices such as laser, LED, UV filters, radiation detection and measurement, and optical fibres (Abdullahi et al., 2019; Bulus et al., 2019; Gonçalves et al., 2018). Better improved transition, the solubility of REI, bandwidth, low cost and easy fabrication technology make glasses more attractive relative to crystals (Yamusa et al., 2018). Absorption and emission behaviour of REI activated glasses depend to some extent on the host former and incorporated modifiers and intermediates (Jupri et al., 2017). Incorporation of transition metals into glass dope with REI found applications in electrical, optical, mechanical as well as probe for glass structure studies (Hegde et al., 2019).

Particularly, borate-based hosts are attractive as they form glass with exceptional transparency, excellent acceptability of REI, thermal stability with comparatively lower melting temperature (Rani et al., 2019). Nd^{3+} doped glasses are prospective photonic and optical materials, for application in solid states lasers and waveguides, refractory glass and band rejection filter due to their good mechanical and chemical durability (Ahmad et al., 2019). Nd^{3+} doped in different glass formers such as borate (Zaman et al., 2016), chalcogenides (Lima et al., 2001), fluorides (Manasa et al., 2017), germanate (Veeranna Gowda, 2015), phosphate (Algradee et al., 2017), silicate (Pal et al., 2014) and tellurite (Kumar et al., 2018) are reported. However, Nd^{3+} ions activated borate glass modified with lithium and strontium with zinc as intermediate has never been reported based on the existing literature.

Considering the significance of REIs doped borate-based amorphous hosts, a series of $20Li_2CO_3$–5SrO–5ZnO–(70-x)B_2O_3–xNd_2O_3 ($0 \leq x \leq 2$) glasses were prepared using the melt-quenching procedure. The glass samples were analysed using XRD, and EDX to ascertain their amorphous nature and elemental composition, respectively. The optical absorption spectra recorded at room temperature were analyzed in the light of the ligand field: crystal field and nephelauxetic effects from the Nd^{3+} dependent optical absorption spectra.

2.0 Experimental Procedure

2.1 Sample Preparation

The Nd^{3+} activated borate-based glasses with composition of $20Li_2CO_3$–5SrO–5ZnO–(70-x)B_2O_3– x Nd_2O_3 (x = 0, 0.4, 0.8, 1.2, 1.6 and 2.0) were developed by employing the universal melt-quenching technique from the analytical grade (Sigma Aldrich) chemical materials viz. Li_2CO_3, SrO, ZnO, B_2O_3, and Nd_2O_3. The weighted powdered chemicals were thoroughly mixed in an agate mortar to make the mixture homogenous. The homogeneous chemical mixture was placed in an aluminium made crucible and then transferred to an electric furnace at 1200 ^oC at an ambient condition for 1 h. The melt was quenched onto a pre-heated brass plate at 300 ^oC and annealed for 3 h to circumvent embrittlement of the samples. The glass eventually settled down to room temperature. Based on the concentrations of the Nd^{3+} ions, the as-quenched glass samples were given code as LSZBNd0.0, LSZBNd0.4, LSZBNd0.8, LSZBNd1.2, LSZBNd1.6, LSZBNd2.0.

2.2 Characterization Tools

The as-prepared samples were chemically stable, non-hygroscopic and transparent. The amorphous nature of the glasses was verified using X-ray diffractometer (Rigaku smart-lab) which is coupled with diffraction software. The diffractometer worked at 40 kV, 30 mA and an angular scan of (2θ) in the interval of 0 to 100^o. The elemental composition of the glasses was detected via Energy Dispersive X-ray (EDX) analysis by employing the services of variable pressure scanning electron microscope (X-MaxN100TLE model) operated at 0–20 keV energy interval. Shimadzu 3600plus Spectrometer with spectral resolution of $\pm$0.1 nm was used to record the optical absorption spectra of the glasses at room temperature.

3. Results and Discussion

3.1 XRD Pattern and EDX Spectra

Figure 1 presents XRD pattern of the LSZBNd0.0 and LSZBNd1.2 samples. The pattern reveals a broad hump between 15o and 38o with no sharp diffraction peak. This indeed confirmed that the studied glass samples are amorphous in nature. Figure 2 illustrates (a) scanning electron microscopy image (b) Spectrum of energy dispersive X-ray and (c) EDX maps of LSZBNd1.2 sample. The SEM image indicates surface which is smooth and homogeneous with no grain borders. The EDX spectrum confirms the presence of O, Sr, Zn, B and Nd elements. However, the element Li could not be detected in the samples due to the facts that the Li K-shell X-ray radiation has very low energy which is too little to be detected by EDX (Nurhafizah et al., 2017). The EDX layers shows the presence of Al in the glass sample which is not in the composition. The present of Al in the sample is attributed to the contamination from the Aluminum.

3.2 Optical Absorption Spectra

Figure 3 present the spectra of the optical absorption of the studied glasses. The spectra depict twelves peaks in the wavelength interval of 300 to 950 nm corresponding to the transitions from the ground state of $^4I_{9/2}$ to the various excited states of ($^4D_{1/2}$ $^4D_{5/2}$ $^4D_{3/2}$), $^2P_{1/2}$, $^4G_{11/2}$, $^2K_{15/2}$, $^4G_{9/2}$, $^4G_{7/2}$, $^4G_{5/2}$, $^2H_{11/2}$, $^4F_{9/2}$, ($^4F_{7/2}$ $^4S_{3/2}$), $^4F_{5/2}$ and $^4F_{3/2}$. These transitions correspond to wavelength (nm) of 353, 429.5, 461.5, 473.5, 512.5, 524.5, 580.5, 625, 679, 744, 801 and 873.5, respectively. The most intense transition (hypersensitive) satisfies the quadrupole selection rule $|\Delta S| = 0$, $|\Delta L| \leq 2, |\Delta J| \leq 2$ was observed at 581 nm (Hehlen et al., 2013; Walsh, 2016). The reported spectra in this

communication are in tandem with those reported in the state of art literature (Lukaszewicz et al., 2021; Venkateswarlu et al., 2021 and Yusof et al., 2020).

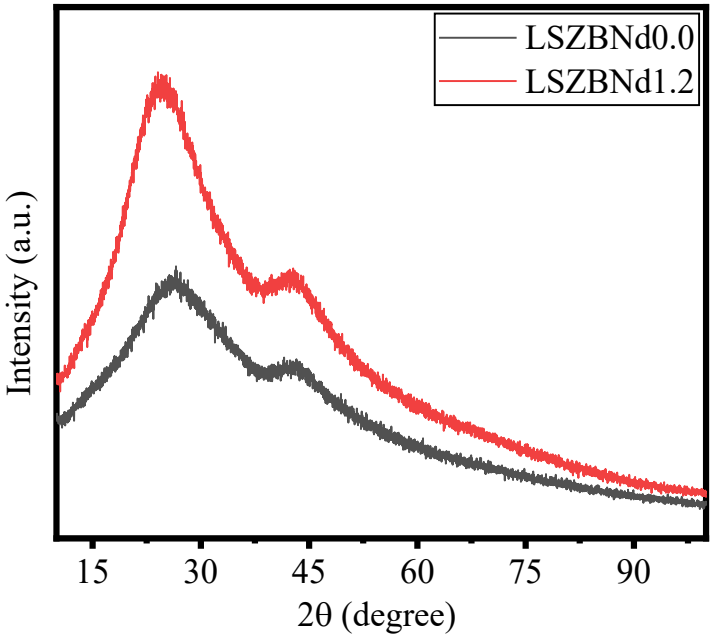

Figure 1. XRD spectra of LSZBNd0.0 and LSZBNd1.2 samples

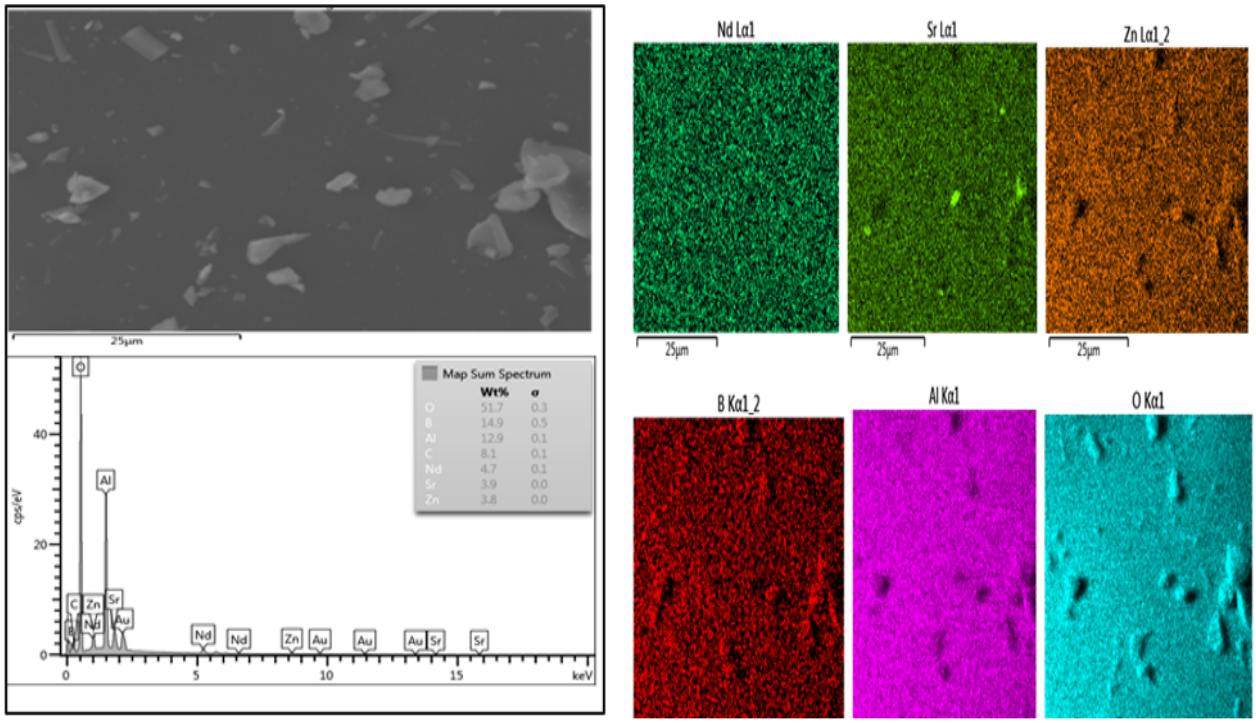

Figure 2. (a) SEM image, (b) EDX spectrum and (c) EDX map showing the constituent elements of the LSZBNd1.2 sample

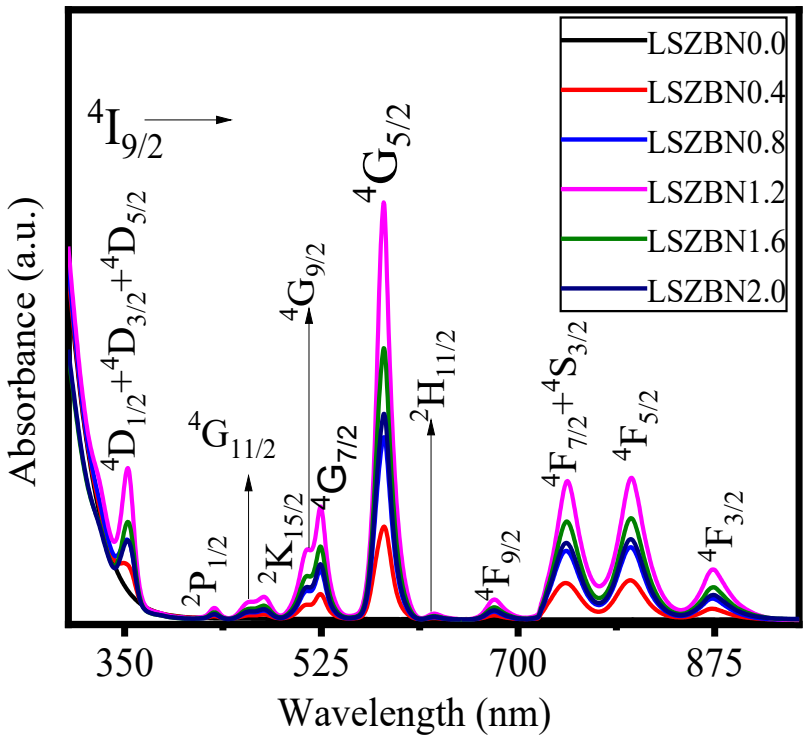

Figure 3. Optical absorption spectra of the prepared glasses

Table 1 enlists nephelauxetic ratio (β), bonding parameter (δ), Racah parameters (B, C) the crystal field strength Dq and D_q/B of the proposed glasses. The nephelauxetic ratio and the bonding parameter which were determined via Equation 1 and 2 respectively (George et al., 2019).

$$\beta = \frac{\upsilon_c}{\upsilon_a} \quad (1)$$

$$\delta = \left(\frac{1-\bar{\beta}}{\bar{\beta}}\right) x\ 100 \quad (2)$$

where $\bar{\beta} = \frac{\sum_n \beta}{N}$, υ_c are the wavenumbers if the respective transitions of the samples, υ_a represents energies (wavenumbers) of the equivalent transition in the aqua solution and N is the considered transitions. The nephelauxetic ratio pattern indicates little change in the Nd^{3+}–O bond with the increase in Nd_2O_3. The negative value of δ recorded indicates ionic nature of the bond between neodymium and oxygen in the present glass composition (Gokce & Kocyigit, 2019).

Figure 4 shows the region of higher energy absorption spectra from which ligand field parameters are generated, crystal field strength using Equation 3 while Racah parameters using Equation 4 and 5 respectively (Danmallam et al., 2019).

$$D_q = \frac{\upsilon_1}{10} \quad (3)$$

$$B = \frac{2\upsilon_1^2+\upsilon_2^2+3\upsilon_1\upsilon_2}{15\upsilon_2-27\upsilon_1} \quad (4)$$

$$C = \frac{\upsilon_3-4B-10D_q}{3} \quad (5)$$

where v_1, v_2 and v_3 are the first three absorption bands found in lower wavelength section of the absorption spectra. The D_q values disclosed reasonable change signifying changes in the crystal field of the samples with the Nd_2O_3 content. The increase in the of Racah parameters further suggest that the nature of the interaction between Nd^{3+} and their surrounding is ionic (less covalent) (Danmallam et al., 2019).

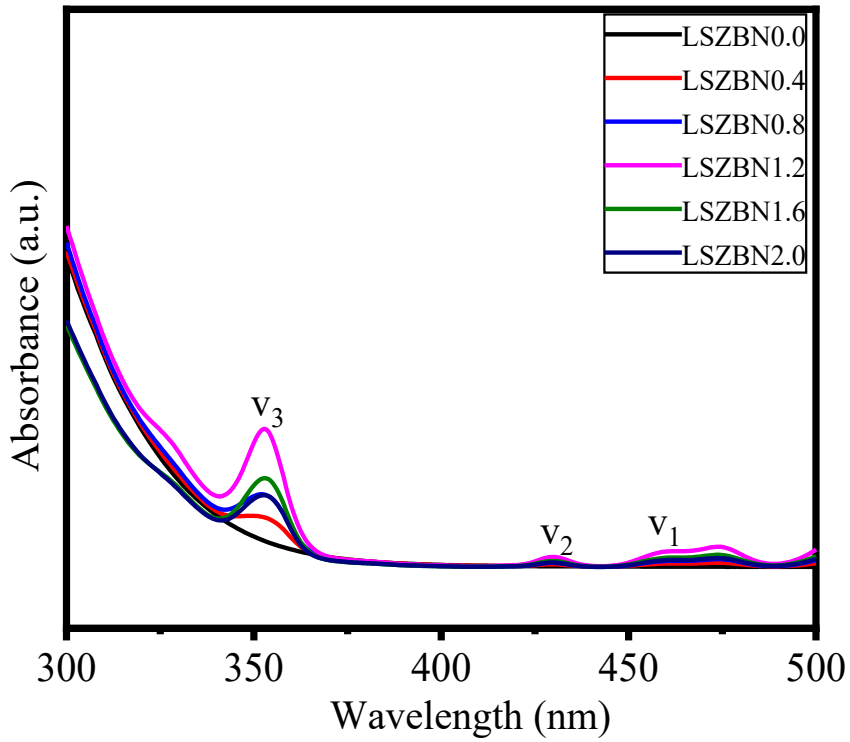

Figure 4. Lower wavelength section of optical absorption spectra of the glasses

Table 1. Nephelauxetic ratio (β), bonding parameter (δ), Racah parameters (B) and (C) and the crystal field strength D_q and D_q/B of the studied glasses

Glass sample	β	δ	B (cm^{-1})	C (cm^{-1})	D_q (cm^{-1})	D_q/B
LSZBNd0.4	12.014	-0.114	131.45	2135	2176	16.56
LSZBNd0.8	12.012	-0.096	135.56	2050	2172	16.02
LSZBNd1.2	12.003	-0.024	137.30	2037	2167	15.78
LSZBNd1.6	12.011	-0.093	135.56	2024	2172	16.02
LSZBNd2.0	12.012	-0.096	133.20	2040	2172	16.30

3.4 Optical Bandgap Energy and Urbach Energy

Figure 5 illustrates the DASF plot ($\frac{d\left\{ln\left[\frac{A(\lambda)}{\lambda}\right]\right\}}{d\left[\frac{1}{\lambda}\right]}$ against $\frac{1}{\lambda}$) showing the discontinuity point at $\frac{1}{\lambda} = \frac{1}{\lambda_g}$ which was generated from Equation 6. Optical band gap and charge carrier transition can be evaluated by substituting the value of $\lambda_g{}^{-1}$ in Equation 7.

$$\frac{d\left\{ln\left[\frac{A(\lambda)}{\lambda}\right]\right\}}{d\left[\frac{1}{\lambda}\right]} = \frac{m}{\lambda^{-1}-\lambda_g^{-1}} \quad (6)$$

$$E_g^{DASF} = \frac{hc}{\lambda_g} = \frac{1239.83}{\lambda_g} \quad (7)$$

where A, λ_g and m are the optical absorbance, point of discontinuity and charge carrier transition index, respectively.

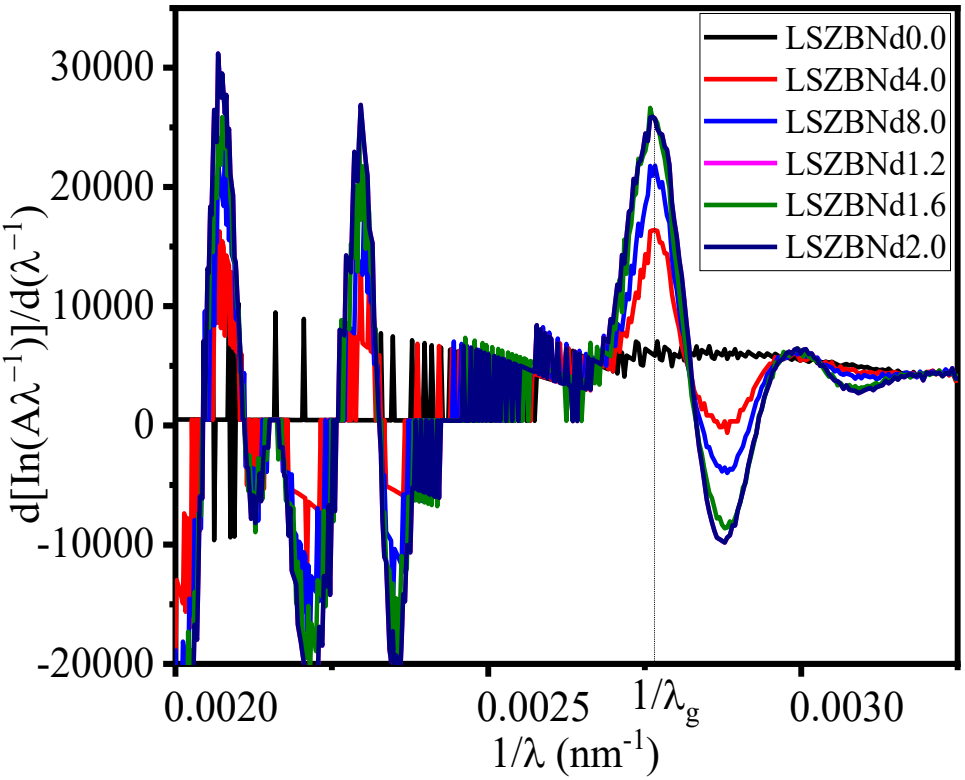

Figure 5. DASF plots of Nd2O3 contnet-dependent showing discontinuity at $1/\lambda_g$

Table 2 shows the Nd_2O_3 concentration-dependent optical band gap and Urbach energies and transition index which were calculated using DASF method. The bandgap decreases with Nd2O3 concentration suggesting structural changes and conversion of BO to NBO (Bulus et al., 2019). The calculated values of the charge transition $m \approx 0.5$ indicate direct allowed, as m indicates the nature of optical transitions. The value of $m = 1/2, 2$ indicates direct, indirect allowed while $m = 3/2\,, 3$ means direct and indirect prohibited transitions respectively (Mariselvam et al., 2019). The obtained value of Urbach energy increases with Nd2O3 content suggesting increase in asymmetry (disorderliness) in the glass system (Mariselvam et al., 2019).

Table 2. Nd_2O_3 content-dependent bandgap and Urbach energies and transition obtained via DASF method

Glass sample	E_g (eV)	Transition m	E_{Tail} (eV)
LSZBNd0.4	3.4284	0.5304	0.9982
LSZBNd0.8	3.4252	0.5277	1.0301
LSZBNd1.2	3.4252	0.6230	1.0661
LSZBNd1.6	3.4238	0.5971	1.1642
LSZBNd2.0	3.4252	0.6553	1.1534

4. Conclusion

This paper reports the synthesis and systematic characterizations of Nd_2O_3 doped lithium strontium zinc borate glasses. Highly transparent, stable, and crack-free glasses were achieved. The glasses optical characteristics, ligand field, crystal field and Racah parameters of studied glasses, were sensitive to the changing Nd^{3+} concentration. The optical band gap obtained through DASF methods revealed the conversion of BO_3 units to BO_4 one as a function of altering Nd_2O_3 contents. Both the ligand field and nephelauxetic ratio and Racah parameters indicated that the Nd^{3+} and the ligand environment bonds were more ionic in character than covalent. The energy band gap indicated direct allowed transition while the decrease in their value signified the conversion of BO to NBO. The achieved optical properties of the glass host could be applicable in photonics devices.

References

Abdullahi, I., Hashim, S., & Ghoshal, S. K. (2019). Waveguide laser potency of samarium doped BaSO4-TeO2-B2O3 glasses: Evaluation of structural and optical qualities. Journal of Luminescence, 216(April), 116686. https://doi.org/10.1016/j.jlumin.2019.116686

Ahmad, A. U., Hashim, S., & Goshal, S. K. (2019). Optical traits of neodymium-doped new types of borate glasses: Judd-Ofelt analysis. Optik, 199, 163515. https://doi.org/10.1016/j.ijleo.2019.163515

Algradee, M. A., Alwany, A. E. B., Sultan, M., Elgoshimy, M., & Almoraisy, Q. (2017). Physical and optical properties for Nd2O3 doped lithium-zinc-phosphate glasses. Optik, 142, 13–22. https://doi.org/10.1016/j.ijleo.2017.05.065

Bulus, I., Hussin, R., Ghoshal, S. K., Tamuri, A. R., & Jupri, S. A. (2019). Enhanced elastic and optical attributes of boro-telluro-dolomite glasses: Role of CeO2 doping. Ceramics International. https://doi.org/10.1016/j.ceramint.2019.06.089

Danmallam, I. M., Ghoshal, S. K., Ariffin, R., Jupri, S. A., & Sharma, S. (2019). Europium ions and silver nanoparticles co-doped magnesium-zinc-sulfophosphate glasses: Evaluation of ligand field and Judd-Ofelt parameters. Journal of Luminescence, 216(August). https://doi.org/10.1016/j.jlumin.2019.116713

George, H., Deopa, N., Kaur, S., Prasad, A., Sreenivasulu, M., Jayasimhadri, M., & Rao, A. S. (2019). Judd-Ofelt parametrization and radiative analysis of Dy3+ ions doped Sodium Bismuth Strontium Phosphate glasses. Journal of Luminescence, 215, 116693. https://doi.org/10.1016/j.jlumin.2019.116693

Gökçe, M., & Koçyiğit, D. (2019). Spectroscopic investigations of Dy3+ doped borogermanate glasses for laser and wLED applications. Optical Materials, 89(February), 568–575. https://doi.org/10.1016/j.optmat.2019.02.004

Gonçalves, T. S., Santos, J. F. M., Sciuti, L. F., Catunda, T., & Camargo, A. S. S. De. (2018). Thermo-optical spectroscopic investigation of new Nd3+-doped fluoro-aluminophosphate glasses. Journal of Alloys and Compounds, 732, 887–893. https://doi.org/10.1016/j.jallcom.2017.10.152

Hegde, V., Chauhan, N., Viswanath, C. S. D., Kumar, V., Mahato, K. K., & Kamath, S. D. (2019). Photoemission and thermoluminescence characteristics of Dy3+-doped zinc sodium bismuth borate glasses. Solid State Sciences, 89, 130–138. https://doi.org/10.1016/J.SOLIDSTATESCIENCES.2019.01.002

Hehlen, M. P., Brik, M. G., & Krämer, K. W. (2013). 50th anniversary of the Judd–Ofelt theory: An experimentalist's view of the formalism and its application. Journal of Luminescence, 136, 221–239. https://doi.org/10.1016/j.jlumin.2012.10.035

Jupri, S. A., Ghoshal, S. K., Omar, M. F., & Sharma, S. (2017). Improved absorbance of holmium activated magnesium-zinc- sulfophosphate glass. Malaysian Journal of Fundamental and Applied Sciences, 13(3), 253–257. https://mjfas.utm.my/index.php/mjfas/article/view/559/pdf

Kumar, J. S., Pavani, K., Gavinho, S. R., Seshadri, M., Anjos, V., Bell, M. J. V., Freire, F. N., Valente, M. A., Soares, M. J., & Graça, M. P. F. (2018). Temperature dependent upconversion and spectroscopic properties of Nd3+doped barium bismuth tellurite glasses. Journal of Non-Crystalline Solids, 498(January), 89–94. https://doi.org/10.1016/j.jnoncrysol.2018.05.031

Lima, S. M., Sampaio, J. A., Catunda, T., de Camargo, A. S. S., Nunes, L. A. O., Baesso, M. L., & Hewak, D. W. (2001). Spectroscopy, thermal and optical properties of Nd3+-doped chalcogenide glasses. Journal of Non-Crystalline Solids, 284(1–3), 274–281. https://doi.org/10.1016/S0022-3093(01)00414-8

Łukaszewicz, M., Klimesz, B., Szmalenberg, A., Ptak, M., & Lisiecki, R. (2021). Neodymium-doped germanotellurite glasses for laser materials and temperature sensing. Journal of Alloys and Compounds, 860(xxxx). https://doi.org/10.1016/j.jallcom.2020.157923

Manasa, P., Ramachari, D., Kaewkhao, J., Meejitpaisan, P., Kaewnuam, E., Joshi, A. S., & Jayasankar, C. K. (2017). Studies of radiative and mechanical properties of Nd3+-doped lead fluorosilicate glasses for broadband amplification in a chirped pulse amplification based high power laser system. Journal of Luminescence, 188(April), 558–566. https://doi.org/10.1016/j.jlumin.2017.04.065

Mariselvam, K., Arun Kumar, R., & Rajeswara Rao, V. (2019). Concentration-dependence and luminescence studies of erbium doped barium lithium fluoroborate glasses. Optics and Laser Technology, 118(February), 37–43. https://doi.org/10.1016/j.optlastec.2019.04.028

Nurhafizah, H., Rohani, M. S., & Ghoshal, S. K. (2017). Self cleanliness of Er3+/Nd3+ Co-do ped lithium niobate tellurite glass containing silver nanoparticles. Journal of Non-Crystalline Solids, 455, 62–69. https://doi.org/10.1016/j.jnoncrysol.2016.10.028

Pal, I., Agarwal, A., Sanghi, S., Aggarwal, M. P., & Bhardwaj, S. (2014). Fluorescence and radiative properties of Nd3+ ions doped zinc bismuth silicate glasses. Journal of Alloys and Compounds, 587, 332–338. https://doi.org/10.1016/j.jallcom.2013.10.191

Rani, P. R., Venkateswarlu, M., Mahamuda, S., Swapna, K., Deopa, N., Rao, A. S., & Prakash, G. V. (2019). Structural, absorption and photoluminescence studies of Sm3+ ions doped barium lead alumino fluoro borate glasses for optoelectronic device applications. Materials Research Bulletin, 110(October 2018), 159–168. https://doi.org/10.1016/j.materresbull.2018.10.033

Veeranna Gowda, V. C. (2015). Physical, thermal, infrared and optical properties of Nd3+ doped lithium-lead-germanate glasses. Physica B: Condensed Matter, 456, 298–305. https://doi.org/10.1016/j.physb.2014.09.004

Venkateswarlu, M., Swapna, K., Mahamuda, S., Rani, P. R., Kumar, J. V. S., Prasad, M. V. V. K. S., & Rao, A. S. (2021). Concentration dependent neodymium doped oxy fluoroborate glasses for 1.08 μm laser applications. Solid State Sciences, 113, 106543. https://doi.org/10.1016/j.solidstatesciences.2021.106543

Walsh, B. M. (2006). Advances in Spectroscopy for Lasers and Sensing (B. Di Bartolo & O. Forte (eds.); Issue December 2005). Springer Netherlands. https://doi.org/10.1007/1-4020-4789-4

Yamusa, Y. A., Hussin, R., & Shamsuri, W. N. N. W. (2018). Physical, optical and radiative properties of CaSO4–B2O3–P2O5glasses doped with Sm3+ions. Chinese Journal of Physics, 56(3), 932–943. https://doi.org/10.1016/j.cjph.2018.03.025

Yusof, N. N., Ghoshal, S. K., & Jupri, S. A. (2020). Luminescence of Neodymium Ion-Activated Magnesium Zinc Sulfophosphate Glass: Role of Titanium Nanoparticles Sensitization. Optical Materials, 109, 110390. https://doi.org/10.1016/j.optmat.2020.110390

Zaman, F., Rooh, G., Srisittipokakun, N., Ruengsri, S., Kim, H. J., & Kaewkhao, J. (2016). Luminescence behavior of Nd3 +-activated soda-lime-borate glasses for solid-state lasers applications. Journal of Non-Crystalline Solids, 452, 307–311. https://doi.org/10.1016/j.jnoncrysol.2016.09.007